

# InGaP@ZnS-Enriched Chitosan Nanoparticles: A Versatile Fluorescent Probe for Deep-Tissue Imaging\*\*

By Marinella G. Sandros, Maik Behrendt, Dusica Maysinger, and Maryam Tabrizian\*

InGaP QDs overcoated with several monolayers of ZnS are covalently bound to chitosan to address the challenges of developing highly biologically stable and fluorescent nanoparticle probes for deep-tissue imaging. Transmission electron microscopy images reveal that the average diameter of these luminescent nanoparticles is approximately 29 nm, and they contain multiple InGaP@ZnS QDs that have an average diameter between 4 and 5 nm. These new InGaP@ZnS–chitosan nanoparticles emit near the near IR region at 670 nm and are able to penetrate three times deeper into tissue (e.g., even through a mouse skull) while revealing a higher uptake efficiency into PC12 cells with a robust signal. Additionally, a cell viability assay demonstrates that these new fluorescent nanoparticles have good biocompatibility and stability with PC12 cells and neural cells. As a result, these near-IR-emitting nanoparticles can be used for real-time and deep-tissue examination of diverse specimens, such as lymphatic organs, kidneys, hearts, and brains, while leaving the tissue intact.

## 1. Introduction

Deep tissue imaging<sup>[1,2]</sup> has been rather difficult and invasive using conventional techniques. In the last ten years, quantum dots (QDs) composed of group II and VI metals, have emerged as potential non-invasive imaging tools in the biomedical field to overcome fast photobleaching. Nevertheless, the toxic effects of II–VI QDs and their ability to penetrate deep into tissue continue to be the main concerns for their applicability in *in vitro* and *in vivo* imaging. Attempts to overcome their toxicity have led to the development of highly coated and luminescent II–VI QDs. However, regardless of which surface encapsulation strategy is used with II–VI QDs, they are still inherently cytotoxic because of the release of heavy metals like cadmium, lead, and selenium.<sup>[3–6]</sup> Furthermore, these inorganic fluorophores emit in the UV-vis and are absorbed within the first few micrometers to a millimeter of tissue thickness by deoxy- and oxyhemoglobin (HbO<sub>2</sub>).<sup>[7]</sup> Ideally, fluorophores

that emit in the near IR (NIR, 650–900 nm) are able to diffuse further into tissue because of minimal absorption from HbO<sub>2</sub> in that optical range.<sup>[7]</sup> Recently, there have been numerous reports<sup>[8–10]</sup> describing successful *in vivo* NIR fluorescence imaging in living tissue by employing II–VI. Despite their success, it is important to note that II–VI inside biological systems can transfer energy to nearby oxygen molecules to generate reactive oxygen species (ROSs) like hydroxyl radicals, superoxides, and singlet oxygen species, which can then induce cell death.<sup>[11]</sup> On the other hand, III–V QDs are composed of nonheavy metal elements that are known to be less cytotoxic.<sup>[3]</sup> Due to the robustness and strength of their covalent bond in contrast to an ionic bond present in II–VI QDs,<sup>[12]</sup> QD-based fluorescent markers that are capped with small organic molecules suffer from fast degradation and oxidation.<sup>[13]</sup> Researchers resolved this problem by introducing QDs to large polymer microbeads ( $\mu\text{m}$  scale),<sup>[14–16]</sup> which can be used for multiplexed immunoassays but not for subcellular or intracellular imaging because of their large size. Therefore, QD-based fluorescent markers employed in *in vitro* and *in vivo* applications must be on the nanometer scale with a narrow size distribution, a high uptake efficiency, and the ability to penetrate deep into tissue.

Inert poly(ethylene glycol) coated QD (PEG–QD) nanoparticles have improved upon the cytotoxicity of CdSe QDs, but this improvement was mainly the result of the reduced uptake of these nanoparticles into cells.<sup>[17]</sup> Alternatively, negatively charged QDs were complexed with cationic liposomes<sup>[17,18]</sup> or amino-modified, cholesterol-bearing pullulan<sup>[19]</sup> through electrostatic interactions and improved upon the uptake efficiencies of QDs in live cells. Additionally, formation of CdSe@ZnS QD–chitosan nanoparticles via chelation,<sup>[20]</sup> electrostatic interactions,<sup>[21–23]</sup> and covalent binding<sup>[24]</sup> has previously been reported, but they have only demonstrated biocompatibility and application *in vitro*. Herein, a new bioprobe, where InGaP QDs coated with several monolayers of ZnS were covalently

[\*] Prof. M. Tabrizian, Dr. M. G. Sandros  
Department of Biomedical Engineering, Center for Biorecognition and Biosensors, and McGill Institute for Advanced Materials  
McGill University  
3775 University, Montreal, Quebec H3A2B4 (Canada)  
E-mail: maryam.tabrizian@mcgill.ca  
Prof. D. Maysinger, Dr. M. Behrendt  
Department of Pharmacology and Therapeutics  
McGill University  
3655 Promenade Sir-William-Osler, Montreal, Quebec H3G1Y6 (Canada)

[\*\*] This research was funded by the Canadian Institute for Health Research (CIHR), Le Fonds québécois de la recherche sur la nature et les technologies, and the Natural Sciences and Engineering Research Council of Canada (NSERC). We thank Dr. S. Kelly Sears for assistance with TEM.

bound to chitosan (high degree of deacetylation), is reported for the first time to address the challenges of developing highly biologically stable and fluorescent nanoparticle probes for deep-tissue imaging.

Our approach is not only aimed at using chitosan to enhance QD biostability but also to take advantage of numerous interesting properties of chitosan,<sup>[25,26]</sup> particularly its bioadhesive property. In the field of drug delivery therapeutics,<sup>[27,28]</sup> chitosan is used as a vehicle for drug targeting because it controls the release and enhances the uptake efficiency of the drug across epithelial layers. Additionally, because of its positively charged chains, chitosan can electrostatically interact with DNA (negatively charged) and form complexes that can be taken up by cells through endocytosis and even enter the nucleus. This chitosan property is exploited for transfection in various cell types.<sup>[29–31]</sup> This study provides information regarding the preparation, photophysical properties, and function of the new InGaP-enriched chitosan nanoparticles for bioimaging. We show that the chitosan coating enhances the emission band and particle size distribution, modifies the uptake efficiency, and provides the means for wide applicability in biological and life sciences applications.

## 2. Results and Discussion

A schematic illustrating the preparation of chitosan-capped InGaP@ZnS nanoparticles is shown in Scheme 1. The emission spectra of solutions of mercaptohexadecanoic acid (MHA)-capped InGaP@ZnS QDs and chitosan nanoparticles encapsulated with QDs are compared in Figure 1. The emission band of the QDs embedded in chitosan displayed a 15 nm red-shift with respect to the emission band of the free QDs. This substantial red-shift can be attributed to a change in the surface charge states of the QDs or to a change in the refractive index of the medium surrounding the QDs, which is caused by the presence of chitosan.<sup>[32]</sup> In addition, the full-width at half maximum (FWHM) varied from 75 to 60 nm because of changes in the particle size distribution. The fluorescence quantum yield of InGaP@ZnS QDs was not changed after the addition of chitosan. The quantum yield was determined by comparing the

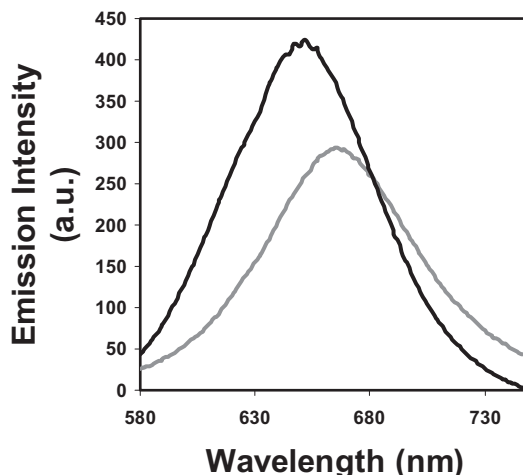
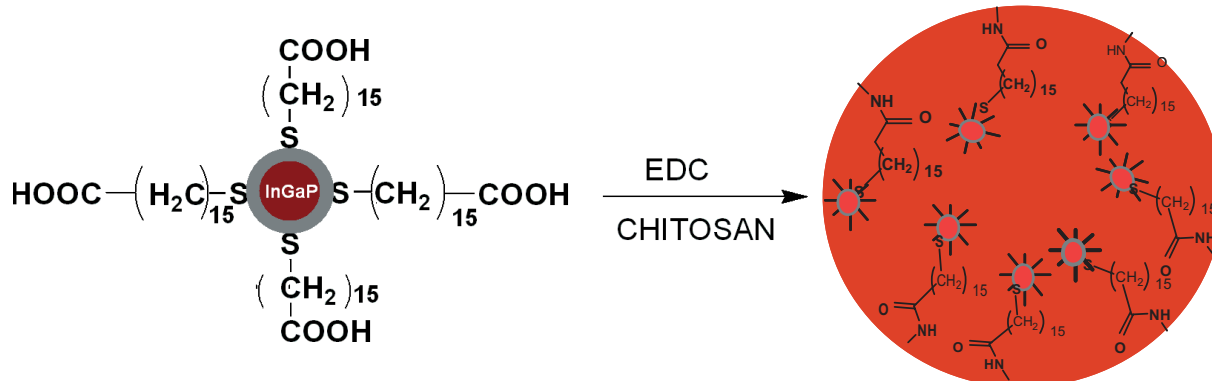


**Figure 1.** Emission spectra of MHA-capped InGaP@ZnS QDs (black line) and chitosan-encapsulated MHA-capped InGaP@ZnS nanoparticles (grey line). No change in quantum yield was observed for the samples when compared to rhodamine 6G (reference standard).

integrated fluorescence intensity of the sample solution to the standard solution (rhodamine 6G) at an excitation wavelength of 488 nm. Quantum yields were calculated as the ratio of the integrated fluorescence intensity of each sample to the intensity of a standard solution and then multiplied by the standard published<sup>[33]</sup> quantum yield value (90 % in H<sub>2</sub>O for rhodamine 6G). The intensity differences between free QDs and chitosan–QD nanoparticles resulted from different concentrations of emitting particles and not from the quenching of the emission quantum yield.<sup>[34]</sup>

Transmission electron microscopy (TEM) was employed to confirm that the InGaP@ZnS QDs were encapsulated within chitosan nanoparticles. Figure 2 shows TEM images of chitosan nanoparticles. An accumulation of InGaP@ZnS QDs is seen as dark spots because of their higher contrast. A higher magnification image of a single chitosan nanoparticle encapsulating multiple (12–16) InGaP@ZnS QDs, each having a diameter of 4–5 nm, can be seen in the inset. The statistics for more than 140 nanoparticles (shown in Fig. 3) are indicative of a



**Scheme 1.** A schematic illustrating the preparation of chitosan-encapsulated MHA-capped InGaP@ZnS.

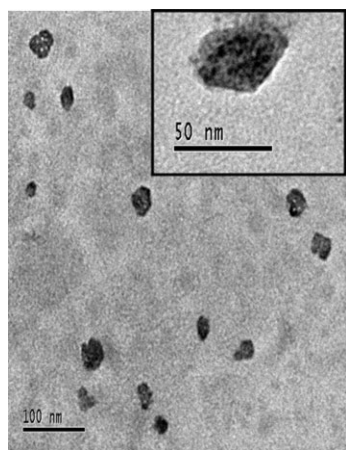


**Figure 2.** TEM micrographs of chitosan-encapsulated MHA-capped InGaP@ZnS nanoparticles at a magnification of 100 X and (inset) 400 X.

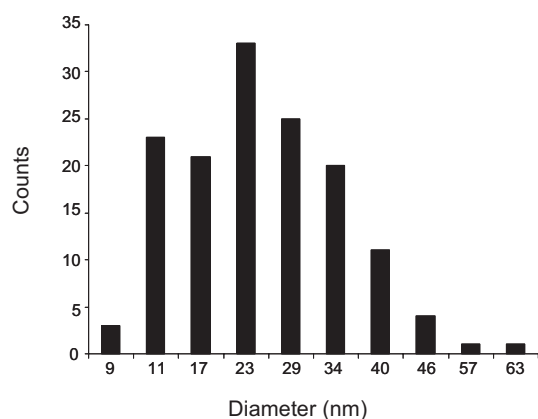


**Figure 3.** Statistical analysis of chitosan-InGaP@ZnS nanoparticle diameters, as evaluated from TEM images of 142 nanoparticles.

particle diameter with a mean value equal to 28.9 nm and a standard deviation of 11.2 nm. It is worth noting that our QD-chitosan nanoparticles were 50% smaller than particles from a previous study<sup>[24]</sup> and were also more distinguishable within the chitosan nanoparticle.

Spectroscopic conformation of the covalent linkage of the MHA-capped InGaP@ZnS QDs to the chitosan was made by using solution-phase <sup>1</sup>H NMR and Fourier transform (FT) IR spectroscopy (Figs. 4 and 5). As expected, the characteristic NMR spectrum (Fig. 4a) for the chitosan polymer in CD<sub>3</sub>COOD/D<sub>2</sub>O exhibited the expected signals for the protons of D-glucosamine in the range 3.0–4.0 ppm and the methyl residue of the N-acetyl at 2.0 ppm. In the case of the MHA-capped InGaP@ZnS, we observed (Fig. 4b) aliphatic signals between 0.8 and 2.5 ppm. Interestingly, upon covalently linking the QDs to chitosan, the corresponding <sup>1</sup>H NMR spectrum (Fig. 4c) indicated the proton near the free amine on the D-glucosamine decreased in peak intensity and shifted downfield from 3.0 to 3.7 ppm because of the deshielding effect induced by the formation of the amide bond. The rest of the protons on the D-glucosamine were shifted slightly upfield along with the

methyl residue on the N-acetyl. All of the aliphatic protons were shifted downfield because of the deshielding from the chitosan polymer. Further verification of the amide bond formation is seen in the FTIR spectra (Fig. 5), where the distinct carbonyl secondary amide band at 1540 cm<sup>-1</sup> increased in intensity, whereas the C–O–C vibrational mode decreased in intensity after addition of the QDs.<sup>[35]</sup>

Favorable photophysical properties of InGaP@ZnS-chitosan nanoparticles compared to the bare InGaP@ZnS QDs have led to biological experiments to ascertain their effects on cell viability and the potential for *in vivo* imaging. InGaP@ZnS-chitosan nanoparticles were tested in cell cultures, and their compatibility was compared with commercial PEG-QD 545. Cell counting after exposure to both types of QDs (20 nm) in different cell types grown in the presence of serum for 24 h clearly showed no significant reduction in cell viability. Additionally, the nanomolar concentration of InGaP@ZnS-chitosan detected inside the cells did not significantly reduce the viability of pheochromocytoma cells (PC12) cells (Fig. 6) or neural cells in the chemically defined medium in the absence of serum. An alamar blue assay was used to measure the cell viability in the presence of QDs, where an enhancement in fluorescence signified healthy cells and a significant reduction in fluorescence represented functionally impaired cells. The viability of PC12 cells treated with InGaP@ZnS (104.17 ± 7.04) %, InGaP@ZnS-chitosan (101.02 ± 3.89) %, or QD-PEG 545 (108 ± 1.59) % was not significantly different from the untreated control (100 %). Moreover, after the exposure of InGaP and InGaP@ZnS-chitosan (10 nm) QDs to mouse primary cortical cultures for 24 h, the total fluorescence of naive (control) cells taken as 100 % was not significantly different from InGaP (92.45 ± 5.2) and InGaP-chitosan-treated cultures (93.41 ± 13.59).

Depending on the biological application, different types of QDs are needed. For example, for tracking stem cells and cell division or addressing the question of intracellular distribution of QDs, the nanoparticles must be highly fluorescent, small, and should be internalized. In contrast, for imaging plasma membrane receptors (e.g., number, site, clustering) with QD-labeled ligands, cell uptake is not desirable. In this case even relatively large QDs are suitable. However, to study the dynamics of the internalization process of ligand-conjugated QDs as well as their intracellular fate, the QDs must be highly fluorescent and small and should efficiently be taken up by cells. Therefore, fluorescence-activated cell sorting (FACS) was used to study the optical properties of these new nanoparticles within PC12 cells. InGaP@ZnS-chitosan nanoparticles were found to internalize into PC12 cells ten times more than the PEG-QDs (Fig. 7). Therefore, these InGaP@ZnS-enriched chitosan nanoparticles are more ideal and efficient probes for labeling cells. Additionally, Figure 8F shows that labeling with chitosan-InGaP@ZnS nanoparticles was more uniform across a large population of cells in comparison to bare InGaP@ZnS QDs (Fig. 8C), as indicated by the narrower width of the cytometry peak at 695 nm. The data suggest that these InGaP@ZnS-enriched chitosan nanoparticles have an advantage of being a more suitable probe for application in multiplex detection assays.

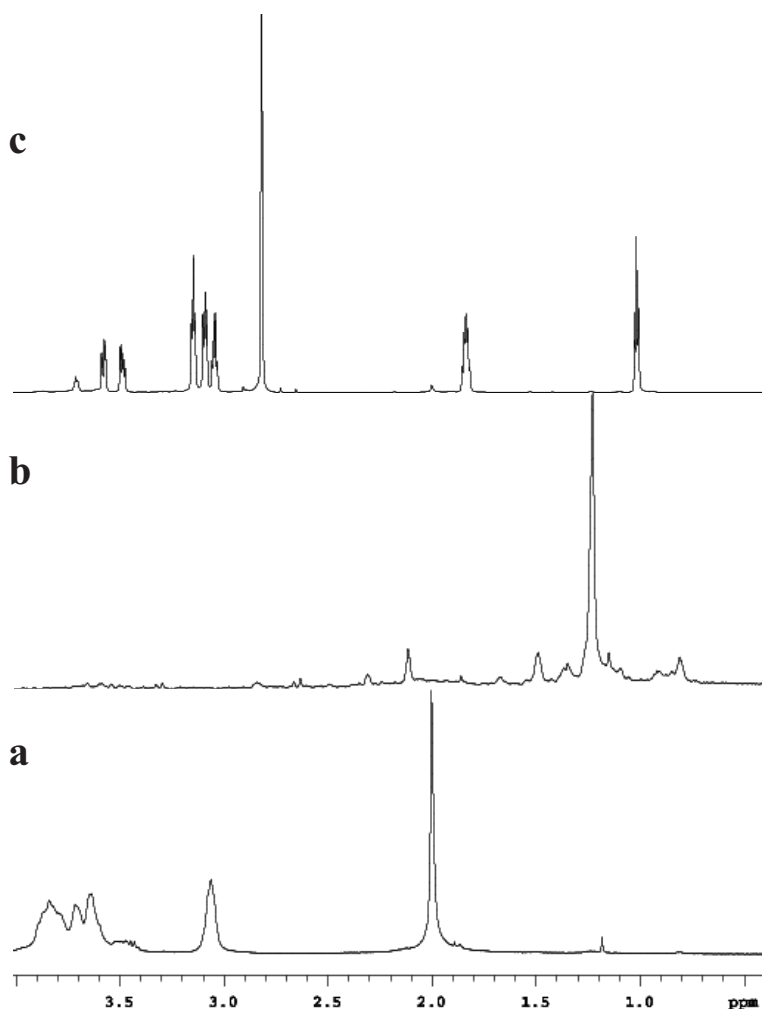


**Figure 4.**  $^1\text{H}$  NMR spectra for a) chitosan polymer, b) MHA-capped InGaP@ZnS QDs, and c) MHA-capped InGaP@ZnS QDs encapsulated in chitosan. The chitosan sample was analyzed in  $\text{CD}_3\text{COOD}/\text{D}_2\text{O}$ , and the QD samples were analyzed in  $\text{D}_2\text{O}$ .

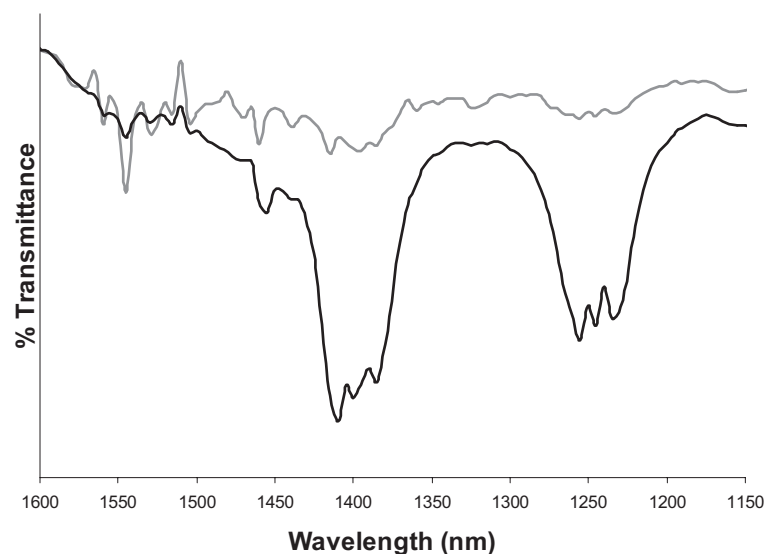


**Figure 5.** FTIR spectra of chitosan (black) and chitosan-capped InGaP@ZnS (grey).

Further, by carrying out experiments with a phantom and Advanced Research Technologies, Inc. (ART) imaging system developed for *in vivo* live animal imaging, we demonstrated the superiority of these new QDs compared to commercially available ones for bioimaging (Fig. 9). The maximum penetration of the luminescent signals from the InGaP@ZnS–chitosan nanoparticles ( $5\ \mu\text{L}$ ) was determined for different distances from zero (i.e., surface) up to 10 mm in depth. Results showed a strong signal from the surface corresponding to the 97218 arbitrary luminescence units. This intensity exceeded the background by more than tenfold even at the lowest laser power ( $5\ \mu\text{W}$ ). Strong signals, decreasing linearly, were detectable up to 6 mm in depth with a limit of 8 mm below the phantom surface, however, at higher laser power settings. In contrast to InGaP@ZnS–chitosan nanoparticles, commercial PEG–QD nanoparticles were not detectable below 2 mm using the same settings and equivalent concentrations (Fig. 9e and f).

More interestingly, results from imaging the brain of live mice injected with InGaP@ZnS–chitosan nanoparticles ( $5\ \mu\text{L}$ ; Fig. 9a–d; 6 mm below the head surface) showed that the signal was detectable even through the skull (Fig. 9g and h). One can conclude from these results that these new InGaP@ZnS–chitosan nanoparticles are highly appealing imaging tools for deep tissue imaging. In addition, these InGaP@ZnS–chitosan nanoparticles can undergo further surface modifications with other chitosans and/or counterion biomolecules.

### 3. Conclusions

We have developed biocompatible chitosan nanoparticles covalently bound to multiple InGaP@ZnS QDs, producing noncytotoxic and long-wavelength-emitting fluorescent probes. To ensure that the chitosan–QD nanoparticles will not break down in the harsh environments found *in vivo*,  $^1\text{H}$  NMR and FTIR verified that these QDs were covalently linked to chitosan. TEM images showed that the chitosan nanoparticles were about 30–50 nm in size and contained multiple InGaP@ZnS QDs. Optical studies revealed upon covalent linkage to chitosan that there was a red-shift in the emission band and a narrowing of the FWHM due to changes in the particle size distribution. Furthermore, a combination of *in vitro* and *in vivo* experiments revealed that chitosan not only functioned as a protective barrier like PEG to reduce oxidation, but it also improved cellular uptake drastically and allowed for deeper tissue penetration than PEG–QD nanoparticles while maintaining cell viability. Therefore, these chitosan–InGaP@ZnS nanoparticle fluorescent probes should open many new

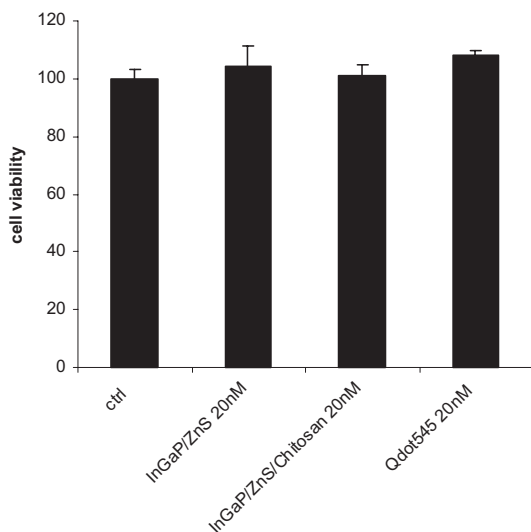


**Figure 6.** Cell viability assay for PC12 cells after 24 h incubation with QDs in a serum-containing medium. Chitosan-capped InGaP/ZnS QDs show similar cell viability compared to the control.

avenues for long-term bioimaging, development of highly sensitive multiplex *in vitro* assays, and *in vivo* cell trafficking studies.

#### 4. Experimental

**Preparation of MHA-Capped QDs:** Trioctylphosphine oxide (TOPO)-capped InGaP@ZnS (Evident Technologies Troy, NY) were exchanged with neat mercaptoalkylcarboxylic acid capping groups such as MHA at 60–70 °C under an inert atmosphere for a couple of hours [36]. The reactants were then dissolved in dimethylformamide (DMF, 300  $\mu$ L) and treated with potassium-*t*-butoxide (0.1 g) to render them negatively charged, hydrophilic QDs. The precipitate was then dispersed in water (10 mL) and centrifuged to remove excess TOPO ligands. To remove residual DMF and excess potassium-*t*-butoxide, the sample was concentrated down to 500  $\mu$ L using ultrafiltration (Amicon, YM-30 membrane) for 10 min. The last step was repeated three times to ensure sample purity.

**Preparation of MHA-QD–Chitosan Composites:** Chitosan (Medipol SA, Switzerland) with a molecular weight of 141 kDa and a degree of deacetylation of 85% was dissolved in a 1% acetic acid solution to a final concentration of 1 mg mL<sup>-1</sup>. To a stirred solution of chitosan (1 mL, 1 mg mL<sup>-1</sup>) was added water-soluble quantum dots (1 mL, 0.1 mg mL<sup>-1</sup>) slowly. The quantum dots were further activated by the slow addition of 1-ethyl-3-(3-dimethylaminopropyl) carbodiimide hydrochloride (EDC, 400  $\mu$ L, 5 mg mL<sup>-1</sup>) and left to react overnight in the dark. The reaction was quenched and purified with 3 cycles of concentration/dilution by ultrafiltration (Nanosep, molecular weight cut-off (MWCO) 300 kDa) for 5 min.

**Characterization of InGaP@ZnS–Chitosan Nanoparticles:** <sup>1</sup>H NMR spectroscopy was performed on a Varian INOVA 800 MHz NMR spectrometer at room temperature. A 2 mg sample of quantum dots was freeze-dried for three days, and 600  $\mu$ L of D<sub>2</sub>O solution was added to it in a 5 mm NMR tube. FTIR spectra were recorded on a Perkin Elmer Spectrum One FTIR fitted with a universal attenuated total

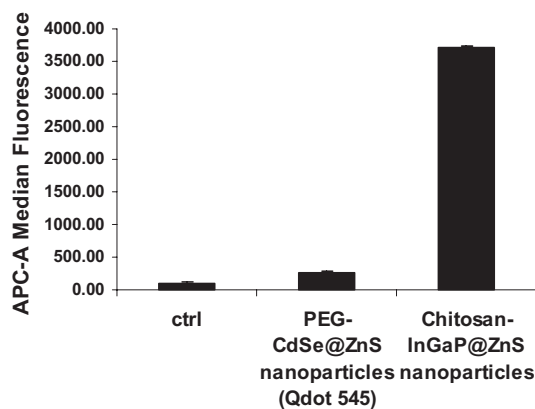


**Figure 7.** A comparison of cellular uptake between chitosan–QD and PEG–QD nanoparticles by FACS in PC12 cells after 24 h incubation.

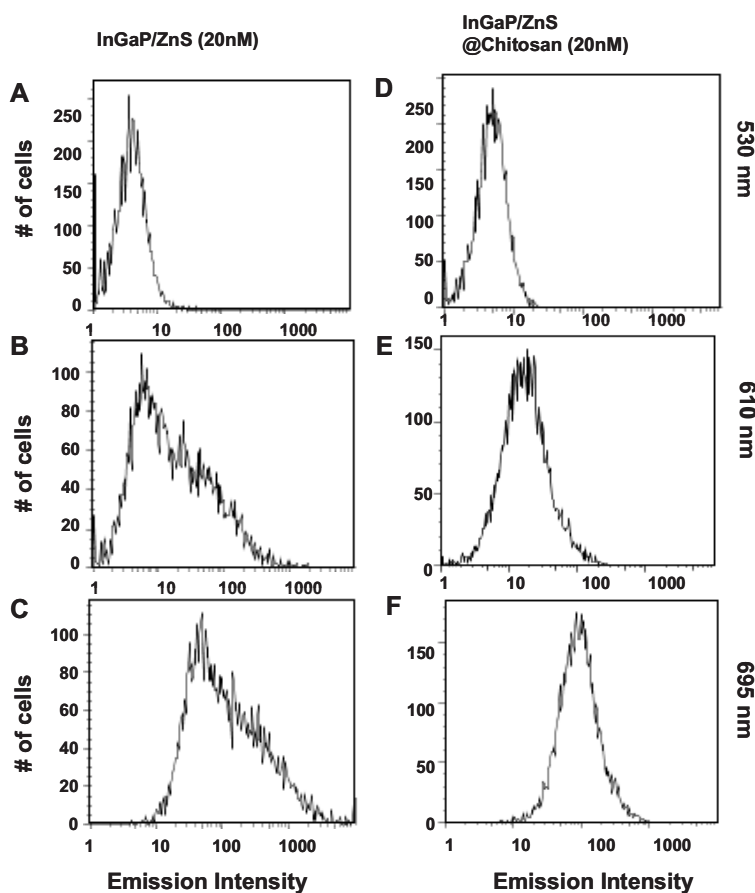


**Figure 8.** Histogram of the fluorescence intensity of PC12 cells with InGaP@ZnS QDs and InGaP@ZnS–chitosan nanoparticles from 530, 610 to 695 nm analyzed by flow cytometry. PC12 cells were incubated with a 20 nM solution of QDs or QD–chitosan nanoparticles for 24 h. a–c) Histogram of bare InGaP@ZnS QDs and d–f) InGaP@ZnS–chitosan nanoparticles. Specific filter sets for determining the emission peaks were used.

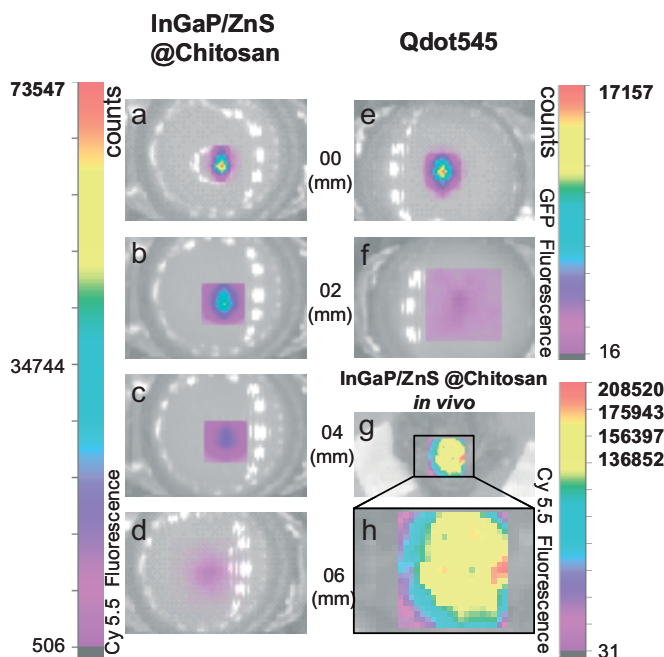


**Figure 9.** Imaging of QDs in tissue-like materials (phantom). A strong detectable signal up to 6 mm for a–d) InGaP@ZnS-chitosan, and e,f) a minimal (4× less) signal to 2 mm at low laser power (5 μW) for QD-PEG 545. g,h) InGaP@ZnS-chitosan has a high detectable signal despite imaging through the skull of a live mouse.

reflectance (ATR) sample analyzer. TEM measurements were performed on a JEOL 2010 microscope operating at 200 kV. The TEM sample was prepared by placing a drop of a dilute sample (1 μm) of InGaP@ZnS-capped chitosan on top of a copper grid, which was left to dry overnight. UV-vis measurements were carried out using a Cary 300 Bio (Varian), and the fluorescence measurements were recorded on a Fluoromax-2 (Horiba Jobin Yvon). Room-temperature photoluminescence quantum yields were determined by comparing the integrated emission of a given InGaP@ZnS QD sample in aqueous solution with that of a fluorescent dye, rhodamine 6G, in aqueous solution.

**Cell Culture:** Rat pheochromocytoma cells (PC12), ATCC number CRL-1721, were maintained at 37 °C in RPMI 1640 medium with L-glutamine supplemented with 5% fetal bovine serum and 1% penicillin-streptomycin. For confocal microscopy, cells were seeded into 8-well chambers Lab-Tek, cat. no. 155411, Nalge Nunc International (10<sup>5</sup> cells cm<sup>-2</sup> colorimetric measurement cells were seeded in 96 well plates, Sarstedt, cat. no. 83.1835).

**Cell Viability Assays:** Colorimetric MTT (3-(4,5-dimethylthiazol-2-yl)-2,5-diphenyl tetrazolium bromide, Sigma) assays were performed to assess the mitochondrial activity of cells treated with InGaP@ZnS-chitosan or QD-PEG 545 (20 μm). After 24 h treatment, the medium were removed and replaced with serum-free medium (500 μL per well). Fifty microliters of stock MTT (5 mg mL<sup>-1</sup>) was added to each well, and cells were then incubated for one hour at 37 °C. The medium was removed, cells were lysed, and formazan was dissolved in dimethylsulfoxide (DMSO). Absorbance was measured at 595 nm using a Benchmark microplate reader (Bio-Rad, Mississauga, ON, Canada). All measurements were done in triplicate in three or more independent experiments.

Cell counting was used as a complementary assessment of cell viability because mitochondrial metabolic activity by itself was not sufficient. Cells were treated in the same way in the MTT assay, and at the end of the experiments, cells were stained with Trypan blue. This dye penetrated only in cells with damaged plasma membranes rendering them blue, whereas viable cells remained clear (unstained). Cell number was assessed by using a Leica microscope with 16× objective. The total

number of viable cells was divided by the total number of cells and expressed as a percentage. The values for untreated controls were considered 100%, and all the other values for the QD-treated cells were expressed relative to these control values. All measurements were obtained in triplicate in three or more independent experiments.

**Determination of Nanoparticle Uptake Using FACS:** For FACS analysis, 10<sup>5</sup> cells were seeded in 24 well plates in RPMI 1640 media containing 10% phosphate-buffered saline (PBS). Twenty-four hours later, the cell culture medium was adjusted to 250 μL per well. PEG-CdSe@ZnS (10 nm), InGaP@ZnS@Chitosan nanoparticles (10 nm, 20 nm), InGaP@ZnS QDs (20 nm), and a control (CdSe@ZnS (bare), 10 nm) were added to the cell culture and incubated for 24 h. After QD incubation, cells were washed twice in PBS. PC12 cells were detached by 0.25% Trypsin/1 mM ethylenediaminetetraacetic acid (EDTA), and the enzymatic reaction was stopped by adding RPMI 1640 media +10% PBS. The PC12 cells were then centrifuged at 2500 rpm for 6 min, resuspended in cold PBS with 1% bovine serum albumin (BSA), and finally stored on ice. Flow cytometric analysis was done on a triple-laser flow cytometer (BD FACS Area, Becton-Dickinson, CA), and data analysis was performed using the Flowjob Treestar Software (Ashland, Oregon, US).

**Bioimaging:** Advanced Research Technologies, Inc. (ART) developed the eXplore Optix, a fluorescence time-domain (TD) optical molecular imager dedicated to small animals that recovers the size, position, and concentration of fluorescent probes embedded in turbid media with 15–30% accuracy. The device uses an ultrafast pulsed diode laser (PDL) to excite fluorescent probes and a time-correlated single photon counting detection system coupled to a photomultiplier tube (PMT) to recover the amount of emitted fluorescent photons from the animal tissues. The ART imaging system was used for *in vitro* and *in vivo* imaging for several fluorescent dyes. Details of imaging procedure and sensitivity of detection using liquid phantoms and Cy5.5 were recently reported [37,38]. For imaging of InGaP@ZnS-chitosan, filter settings for Cy5.5 were used. The QD 545 filter settings for GFP as configured by ART were employed. The phantom was positioned inside the scanning chamber, secured, and the fluorescence intensities were assessed at different depths from the solution surface (0 mm = surface); the sample holder was gradually immersed up to 10 mm below the turbid solution surface. The first scan was done with low 5 μW laser strength and gradually increased to 750 μW to assess the limits of the detection. Animals (mice, n = 3) were anesthetized according to the approved protocol from the McGill University animal care committee. Mice were given a single injection (5 μL of QDs from a 1 μm stock solution) on the left side, 5–7 mm below the head surface, and imaged immediately. The skin and the bone of the mice were removed to measure the fluorescence intensity using a filter setting for Cy5.5.

**Statistical Analysis:** Data were analyzed using SYSTAT 10 (SPSS, Chicago, IL, USA). Statistical significance was determined by Student's t-test, 1-way ANOVA followed by multiparametric Dunnett's post-hoc test, or 2-way ANOVA. Differences were considered significant where \*p < 0.05.

Received: April 17, 2007

Revised: July 25, 2007

Published online: November 14, 2007

- [1] M. J. Levene, D. A. Dombeck, K. A. Kasichke, R. P. Molloy, W. W. Webb, *J. Neurophysiol.* **2004**, *91*, 1908.
- [2] D. R. Larson, W. R. Zipfel, R. M. Williams, S. W. Clark, M. P. Bruchez, F. W. Wise, W. W. Webb, *Science* **2003**, *300*, 1434.
- [3] A. M. Derfus, W. C. W. Chan, S. N. Bhatia, *Nano Lett.* **2004**, *4*, 11.
- [4] R. Hardman, *Environ. Health Perspect.* **2006**, *114*, 165–172.
- [5] A. Shiohara, A. Hoshino, K. Hanaki, K. Suzuki, K. Yamamoto, *Microbiol. Immunol.* **2004**, *48*, 669.
- [6] M. Green, E. Howman, *Chem. Commun.* **2005**, 121.
- [7] P. Sharma, S. Brown, G. Walter, S. Santra, B. Moudgil, *Adv. Colloid Interface Sci.* **2006**, *123–126*, 471.
- [8] S. Kim, Y. T. Lim, E. G. Soltész, A. M. De Grand, J. Lee, A. Nakayama, J. A. Parker, T. Mihaljevic, R. G. Laurence, D. M. Dor, L. H. Cohn, M. G. Bawendi, J. V. Frangioni, *Nat. Biotech.* **2004**, *22*, 93.

- [9] M.-K. So, C. Xu, A. M. Loening, S. S. Gambhir, J. Rao, *Nat. Biotech.* **2006**, *24*, 339.
- [10] Y. Taik Lim, S. Kim, A. Nakayama, N. E. Stott, M. G. Bawendi, J. V. Frangioni, *Mol. Imag.* **2003**, *2*, 50.
- [11] M. L. Christof, M. N. Binil Itty Ipe, *Small* **2005**, *1*, 706.
- [12] D. V. Talapin, N. Gaponik, H. Borchert, A. L. Rogach, M. Haase, H. Weller, *J. Phys. Chem. B* **2002**, *106*, 12 659.
- [13] A. M. Smith, H. Duan, M. N. Rhyner, G. Ruan, S. Nie, *Phys. Chem. Chem. Phys.* **2006**, *8*, 3895.
- [14] M. Han, X. Gao, J. Z. Su, S. Nie, *Nat. Biotech.* **2001**, *19*, 631.
- [15] X. Gao, S. Nie, *Anal. Chem.* **2004**, *76*, 2406.
- [16] P. O'Brien, S. S. Cummins, D. Darcy, A. Dearden, O. Masala, N. L. Pickett, S. Ryley, A. J. Sutherland, *Chem. Commun.* **2003**, 2532.
- [17] A. M. Derfus, W. C. Chan, S. N. Bhatia, *Adv. Mater.* **2004**, *16*, 961.
- [18] S. Hsieh, F. Wang, C. Lin, Y. Chen, S. Hung, Y. Wang, *Biomaterials* **2006**, *27*, 1656.
- [19] U. Hasegawa, S.-I. M. Nomura, S. C. Kaul, T. Hirano, K. Akiyoshi, *Biochem. Biophys. Res. Commun.* **2005**, *331*, 917.
- [20] M. Xie, H.-H. Liu, P. Chen, Z.-L. Zhang, X.-H. Wang, Z.-X. Xie, Y.-M. Du, B.-Q. Pan, D.-W. Pang, *Chem. Commun.* **2005**, 5518.
- [21] W. B. Tan, N. Huang, Y. Zhang, *J. Colloid Interface Sci.* **2007**, *310*, 464.
- [22] D. K. Chatterjee, Y. Zhang, *Sci. Technol. Adv. Mater.* **2007**, *8*, 131.
- [23] W. B. Tan, Y. Zhang, *J. Biomed. Mater. Res. A* **2005**, *75A*, 56.
- [24] Q. Nie, W. B. Tan, Y. Zhang, *Nanotechnology* **2006**, *17*, 140.
- [25] T. Chandy, C. P. Sharma, *Biomater. Artif. Cells Artif. Organs* **1990**, *18*, 1.
- [26] C. M. Lehr, J. A. Bouwstra, E. H. Schacht, H. E. Junginger, *Int. J. Pharm.* **1992**, *78*, 43.
- [27] K. L. Douglas, T. M., *J. Biomater. Sci. Polym. Ed.* **2005**, *16*, 43.
- [28] S. A. Agnihotri, N. N. Mallikarjuna, T. M. Aminabhavi, *J. Controlled Release* **2004**, *100*, 5.
- [29] E. Patrick, Z. Shaomin, B. Thierry, S. Anne-Marie, R. Jean-Serge, *Pharm. Res.* **1998**, *VI5*, 1332.
- [30] V. L. Truong-Le, J. T. August, K. W. Leong, *Human Gene Therapy* **1998**, *9*, 1709.
- [31] T. Ishii, Y. Okahata, T. Sato, *Biochim. Biophys. Acta - Biomembranes* **2001**, *1514*, 51.
- [32] L. M. Liz-Marzan, M. Giersig, P. Mulvaney, *Langmuir* **1996**, *12*, 4329.
- [33] D. Magde, R. Wong, P. G. Seybold, *Photochem. Photobiol.* **2002**, *75*, 327.
- [34] Y. Chen, T. Ji, Z. Rosenzweig, *Nano Lett.* **2003**, *3*, 581.
- [35] M. Mucha, J. Piekilma, A. Wiczorek, *Macromol. Symp.* **1999**, *144*, 391.
- [36] M. G. Sandros, D. Gao, D. E. Benson, *J. Am. Chem. Soc.* **2005**, *127*, 12 198.
- [37] G. Ma, P. Gallant, L. McIntosh, *Appl. Opt.* **2007**, *46*, 1650.
- [38] J. C. Hebden, S. R. Arridge, A. P. Gibson, *Phys. Med. Biol.* **2005**, *50*, R1.